

Article

Effect of Fe Addition on Heat-Resistant Aluminum Alloys Produced by Selective Laser Melting

Shigeto Yamasaki ^{1,*} , Tomo Okuhira ¹, Masatoshi Mitsuhashi ¹, Hideharu Nakashima ¹, Jun Kusui ² and Mitsuru Adachi ³

¹ Faculty of Engineering Sciences, Kyushu University, 6-1 Kasugakoen, Kasuga, Fukuoka 816-8580, Japan; okuhira.tomo.922@s.kyushu-u.ac.jp (T.O.); mitsuhashi@kyudai.jp (M.M.); nakashima.hideharu.792@m.kyushu-u.ac.jp (H.N.)

² Powder & Paste Headquarters, Toyo Aluminium K. K., Osaka 541-0056, Japan; jun-kusui@toyol.co.jp

³ KOIWAI Co., Ltd., Odawara 256-0804, Japan; m-adachi@tc-koiwai.co.jp

* Correspondence: yamasaki.shigeto.259@m.kyushu-u.ac.jp; Tel.: +81-92-583-7524

Received: 26 March 2019; Accepted: 20 April 2019; Published: 22 April 2019



Abstract: The effect of Fe addition on the high-temperature mechanical properties of heat-resistant aluminum alloys produced by selective laser melting (SLM) was investigated in relation to the alloy microstructures. Fe is generally detrimental to the properties of cast aluminum alloys; however, we found that Fe-containing alloys produced by SLM had improved high-temperature strength and good ductility. Microstructural observations revealed that the increase in the high-temperature strength of the alloys was due to the dispersion of fine rod-shaped Fe-Si-Ni particles unique to the SLM material instead of the cell-like structure of eutectic Si.

Keywords: aluminum alloys; selective laser melting; high-temperature deformation; microstructure

1. Introduction

Selective laser melting (SLM) is an additive manufacturing method in which three-dimensional structures are formed by repeated melting and solidification of a metal powder by a laser [1]. SLM has been applied to various metal materials [2]. From a metallurgical perspective, the biggest advantage of SLM is that the cooling rate is much faster than that of the conventional casting method [3], and a characteristic microstructure is formed in the metals and alloys produced by SLM due to rapid solidification. In many studies, SLM has been applied to cast Al alloys containing 10–12% Si [4–9]. The microstructure of these alloys features a half-cylindrical melt pool [4,6] and a eutectic Si cellular structure [4–7] formed by quenching solidification due to the repeated laser scanning melting and solidification. This unique microstructure makes the room-temperature strength of SLM alloys higher than that of cast Al alloys [10,11] or Al alloys made by powder metallurgy [12]. The improvement of the room-temperature strength of Al alloys by SLM has been explained by the cellular structure of fine Si particles [12].

An important mechanical property for engine piston materials that are required to be lightweight to reduce inertia is high-temperature strength to withstand high pressure from combustion gases, even for small parts, as well as wear resistance. Heat-resistant cast Al alloys, obtained by adding an element such as Fe, Ni, Cu, or Mg to an Al–Si alloy near to the eutectic composition, are mainly used as a piston material in automobile engines. The demand for materials that retain their mechanical properties at high temperatures (250–350 °C) is increasing owing to the pressure to improve the efficiency and decrease the emissions of automobile engines. The high-temperature mechanical properties of Al alloys have been improved by optimizing the number of additional elements [13] or adding various elements, such as Mn, Ti, Zr, Sc, or Er, to existing heat-resistant Al alloys [14–16].

Fe is usually present in the Al alloy as an impurity. Fe is detrimental to the properties of cast Al alloys, but an Fe content of about 1 wt % or less is intentionally added to Al die-cast alloys to suppress die soldering [17]. If the cooling rate during casting is slow, the addition of Fe causes coarse plate-like β -Al₅FeSi to crystallize, substantially decreasing toughness [18,19]. However, because Fe has a low diffusion rate in Al, Fe-containing compounds can be used as a dispersion-strengthening phase at high temperatures. Al alloys produced by pressure sintering of rapidly solidified powders containing large amounts of Fe show excellent high-temperature strength [20,21]. Thus, if an extremely high cooling rate is achieved by SLM, it is expected that Al alloys with a high Fe content could be produced without ductility deterioration. Ma et al. [22] prepared an Al-20Si-5Fe-3Cu-1Mg alloy containing 5 wt % Fe by SLM and characterized its microstructure, although they did not evaluate the mechanical properties. In the present work, we used SLM to produce alloys obtained by adding 3–5 wt % Fe to existing heat-resistant Al alloys and evaluated their high-temperature mechanical properties in relation to the alloy microstructure on the conditions assuming application in engine piston materials.

2. Materials and Methods

Table 1 shows the composition of the alloys prepared in this study. The chemical composition of these alloys was based on a conventional heat-resistant alloy AlSi-12CuNiMg (known as AC8A in Japan) and 3% or 5% Fe added to it (in this paper, all percentages for the chemical composition are wt % unless otherwise stated). The sample, equivalent to the chemical composition of the conventional alloy, is referred to as Base alloy, and the samples containing 3% or 5% Fe are referred to as Base + 3Fe or Base + 5Fe, respectively. The SLM alloy powders, which had a true spherical shape as shown in Figure 1, were prepared by atomization at Toyo Aluminium K.K (Hino, Japan). The compositions of the alloy powders are shown in Table 1.

Table 1. Chemical compositions of the alloys (wt %).

Alloy	Al	Si	Cu	Mg	Ni	Fe
Base	bal.	11.6	0.97	0.96	1.0	0.1
Base + 3Fe	bal.	11.6	0.97	0.96	1.0	3.0
Base + 5Fe	bal.	11.6	0.97	0.96	1.0	5.0

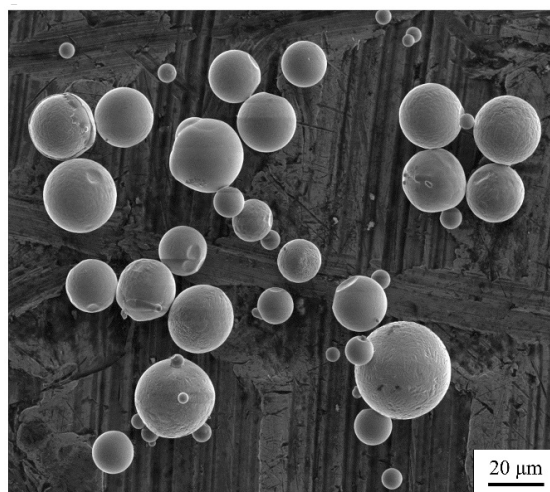


Figure 1. SEM image of the selective laser melting (SLM) powder of Base + 5Fe alloy.

An industrial three-dimensional printer (M280, EOS GmbH, Krailling, Germany) was used for SLM and the details of the manufacturing conditions are summarized in Table 2. Rectangular parallelepipeds of 10 mm × 10 mm × 40 mm or 80 mm (stacking height × width × length) were produced. The energy density, E (J/m³), was calculated by the following formula [23,24]:

$$E = \frac{P}{hvw} \quad (1)$$

where P (J/s) is the laser power, h (m) is the scan line spacing, v (m/s) is the scan rate, and w (m) is the single-layer thickness of the powder. The energy density is the amount of energy of the irradiation beam per unit volume applied to the powder material and is an important condition for producing a sound SLM body. Also, preheating of the substrate was also necessary to suppress destruction of the SLM body during SLM. The conditions summarized in Table 2 are values found to be optimal from prior examinations for producing the SLM bodies of the present alloy.

Table 2. Parameters of selective laser melting.

Powder Size	45 μm
Layer thickness	30 μm
Stacking speed	approx. 3 mm/h
Stacking height	10 mm
Laser beam size	100 μm
Energy density of laser	7.3×10^{10} J/m ³
Preheat temperature	200 °C

In AlSi-12CuNiMg (AC8A), which was the Base alloy in this work, Cu and Mg are added at 1%, so T6 treatment causes age hardening. When this alloy is practically applied to piston materials, it is used after T6 treatment. Therefore, we prepared a T6-treated sample for comparison with conventional materials. A piston material that is used at a high temperature of about 300 °C for a long time is required to have a stable microstructure at the temperature used. In addition, the rapidly solidified SLM material is a highly supersaturated solid solution (SSSS) in the as-built state. Elements are dissolved in the supersaturation precipitate during high-temperature holding, causing dimensional change of the SLM body. In the case of engine pistons, this causes serious problems. Therefore, annealing was performed at 300 °C in order to make the strength and dimensional changes less likely to occur when used for a long time at high temperatures by causing precipitation from an SSSS and growth of precipitates in advance.

Two series of samples with different heat-treatment sequences for the SLM bodies were prepared. In the first series, the samples were annealed at 300 °C after heat treatment equivalent to T6: 510 °C for 2 h (water quenching) followed by 170 °C for 4 h (air cooling). In the second series, the samples were annealed at 300 °C. The annealing details are described later. The first series of samples is called SLM-T6 and the second is called SLM-annealed. For comparison, two series of mold-cast samples made from Base alloy and Base + 3Fe alloy powders were prepared and subjected to the same heat-treatment sequences. The series subjected to T6 heat treatment is called cast-T6, and the series annealed at 300 °C is referred to as cast-annealed. The cast-T6 Base alloy was a sample equivalent to conventional AlSi-12CuNiMg alloy for practical use. All the samples were annealed at 300 °C for 10 h followed by air cooling before processing to a tensile test piece. The samples were sliced into flat plates 10 mm \times 1.5 mm \times 40 mm in size with the plate surface perpendicular to the stacking direction. Then, plates were punched into dog-bone-shaped test pieces with a length of 12 mm and a width of 4 mm for the gauge part. The bending caused by punching was smoothed by grinding. The rough surface of the as-produced SLM material was removed in the sample processing. To remove strain, the tensile test pieces were subjected to additional strain-relieving annealing at 300 °C for 2 h. The heat-treatment history of all the samples is summarized in Figure 2. The grain size of the SLM material after heat treatment was about 20 μm , regardless of the heat-treatment conditions.

The tensile test was carried out at 300 °C. The test piece was placed in an electric furnace, and after holding the furnace temperature at 300 °C for about 1 h, the tensile test was started at a strain rate of 6.9×10^{-3} s⁻¹. The microstructures were characterized by observing the backscattered electron (BSE) images obtained by field-emission scanning electron microscopy (SEM; ULTRA 55, Carl Zeiss, Oberkochen, Germany) and the high-angle annular dark field (HAADF) images obtained

by scanning transmission electron microscopy (STEM; TITAN Cubed G2, FEI, Waltham, MA, USA). Element mapping by energy-dispersive X-ray spectroscopy (EDS) using STEM was also performed. The samples for the SEM observations were finished by colloidal silica polishing. Thin-film samples for the STEM observations were prepared by focused ion beam microsampling.

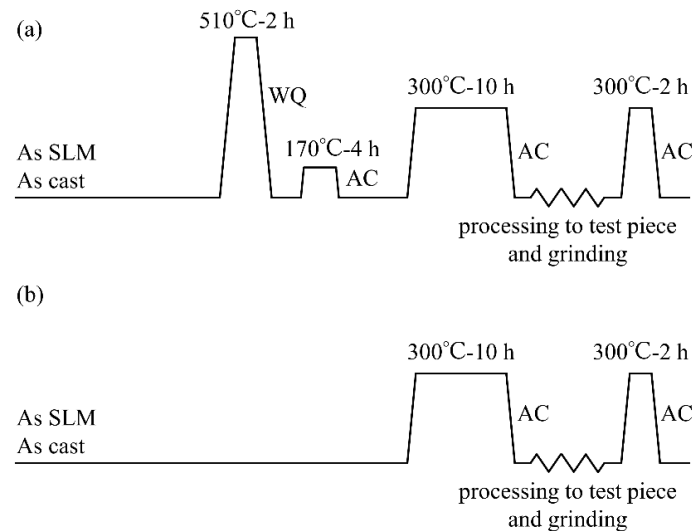


Figure 2. Heat-treatment history of (a) SLM-T6 and cast-T6 and (b) SLM-annealed and cast-annealed.

3. Results and Discussion

Figure 3 shows the true stress–true strain curves of the SLM-annealed, cast-annealed, SLM-T6, and cast-T6 materials at 300 °C. The ultimate tensile strength (UTS) of the SLM-annealed Base alloy was 77 MPa and the elongation to fracture (EL) was about 31%. On the other hand, the UTS and the EL for the cast-annealed Base alloy were 67 MPa and 11%, respectively. The alloy produced by SLM had good ductility but did not differ much from the cast material in high-temperature strength. However, the SLM-annealed Fe-containing alloys showed higher UTS than the SLM-annealed Base alloy at 300 °C. The UTS of the SLM-annealed Base + 3Fe and Base + 5Fe alloys at 300 °C were 165 and 185 MPa, respectively. The UTS increased with the amount of Fe. The UTS of the cast-T6 Base alloy, which can be considered as the conventional AlSi-12CuNiMg alloy, was 94 MPa. The UTS of the SLM-annealed Base + 5 Fe alloy at 300 °C reached about twice that of the cast-T6 Base alloy. The high-temperature strength of the Base alloy produced by casting was increased by the T6 heat treatment. In contrast, for alloys made with SLM, T6 heat treatment caused a reduction in strength. This deterioration of the UTS was remarkable in the Fe-containing alloys.

The UTS and the EL at 300 °C of the sample prepared in this study and the novel cast Al alloys recently reported [25–28] are summarized in Table 3. The UTS at 300 °C of the Fe-added SLM alloys was comparable to that of novel cast Al alloys, the strength of which is improved by the addition of Sr, Ti, Zr, and V. However, it should be noted that UTS at high temperatures depends on the strain rate. Since the strain rate in this study was larger than the literature value, it was considered that UTS was evaluated somewhat higher. The elongation to fracture of the SLM-annealed Base + 3Fe and Base + 5Fe alloy at 300 °C was 20% and 24%, respectively, values which were larger than those of the cast-T6 Base alloy or other novel cast Al alloys [25,26]. The cast Fe-containing alloys were so brittle that the specimens were destroyed when they were punched; thus, the tensile test could not be performed for these materials. When a large amount of Fe is added to cast Al alloys, the coarse plate-shaped β -Al₅FeSi phase crystallizes out. Pores are formed in the material because the molten metal cannot fill the region surrounding the coarse plate-shaped particles [29], and the toughness is degraded. The Fe-containing alloys produced by SLM showed elongation to fracture of at least 20% at 300 °C. Thus, using SLM allowed Fe to be added without impairing toughness. In general, there is

a trade-off between strength and ductility. However, the SLM-annealed Base + 3Fe and Base + 5Fe alloys had high strength and ductility. That is, a material which has a good strength-ductility balance can be produced by using SLM. Similar results have been reported in previous studies and have been explained by the microstructure specific to SLM [11,30].

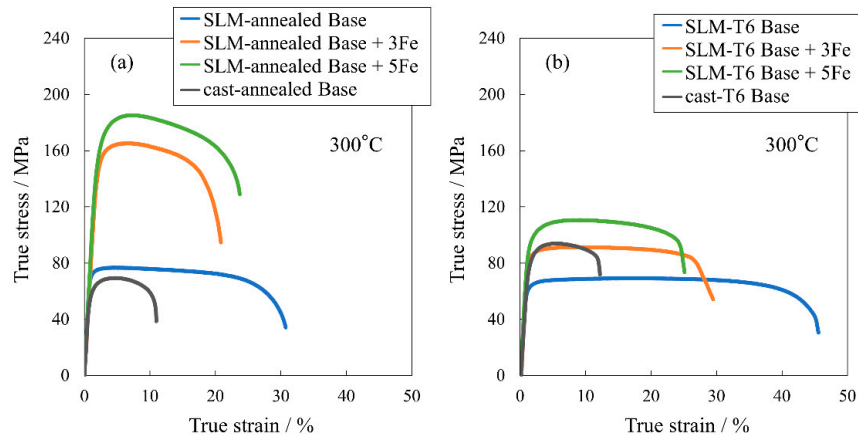


Figure 3. True stress-true strain curves of the SLM material and cast material at 300 °C for (a) SLM-annealed and cast-annealed and (b) SLM-T6 and cast-T6.

Table 3. Summary of the tensile properties at 300 °C.

Alloy	Production Method	Heat Treatment	Strain Rate (s ⁻¹)	UTS (MPa)	EL (%)	Ref.
cast-T6 Base (Al-12Si-1Cu-1Mg-1Ni)	cast	T6 + 300 °C-12 h	6.9×10^{-3}	94	12	This work
SLM-annealed Base	SLM	300 °C-12 h	6.9×10^{-3}	77	31	This work
SLM-annealed Base + 3Fe	SLM	300 °C-12 h	6.9×10^{-3}	165	20	This work
SLM-annealed Base + 5Fe	SLM	300 °C-12 h	6.9×10^{-3}	185	24	This work
Al-7Si-1Cu-0.5Mg-0.1Fe-Sr-Ti-Zr-V	cast	T6	1.3×10^{-3}	132	12	[25]
Al-13Si-5Cu-0.6Fe-0.6Mn-Mg-Ni-Ti-Zr	cast	T6	$\sim 1.7 \times 10^{-3}$	144	7	[26]
Al-9Si-2Cu-0.5Mg-0.2Ni-Sr-Ti-Zr	cast	as cast	4.0×10^{-4}	172	-	[27]
Al-7Si-1Cu-0.5Mg-0.1Fe-Sr-Ti-Zr-V	cast	as cast	1.0×10^{-3}	189	-	[28]

Using SLM with the Base alloy did not dramatically increase the high-temperature strength; however, the Base + 3Fe and Base + 5Fe alloys were strengthened by SLM because of the addition of Fe. The microstructures of these alloys were observed to reveal the reason for the remarkable strengthening by Fe addition. Figure 4 shows the SEM-BSE images of alloys prepared by casting and SLM. In Figure 4, it should be noted that the cast and SLM materials have different scales. In the cast-annealed Base alloy, coarse particles of Chinese script shape or rod shape were observed. These particles were further coarsened by T6 treatment. In the SLM-annealed materials, second-phase particle cells were observed. In the Base alloy, there was a small amount of bright equiaxed particles, whereas in the Fe-containing alloys, there was a large amount of bright rod-shaped particles. In the SLM-T6 materials, both bright equiaxed particles and bright rod-shaped particles were coarsened and no cellular structure was observed.

Figure 5 shows the STEM-EDS mapping of the constituent elements of the second-phase particles in the SLM-annealed Base and Base + 3Fe alloys. In the SLM-annealed Base alloy, Si, Mg, and Cu-Ni particles formed a cellular structure. In the SLM-annealed Base + 3Fe alloy, in addition to these particles, there were many rod-shaped particles consisting mainly of Fe, Si, and Ni. In the EDS element map, particles only enriched with Si were eutectic Si. Eutectic Si is present in cells formed in the Al-Si binary alloy produced by additive manufacturing [4–7]. In the SEM-BSE images (Figure 4), the particles that were slightly brighter than the Al matrix corresponded to eutectic Si. The Si particles in the SLM-annealed materials were about 200 nm in size, whereas the particles were coarsened to several micrometers in the SLM-T6 materials. The bright, equiaxed particles in the SEM-BSE images of the Base

alloy were Cu-Ni particles. Based on the EDS element map, the Fe-Si-Ni particles in the SLM-annealed Base + 3Fe alloy were characteristic rod-shaped particles with a width of 100 nm or less and a length of several hundred nanometers. Based on the shape of the particles, the bright rod-shaped particles in the SEM-BSE images of the Fe-containing alloys corresponded to these Fe-Si-Ni particles.

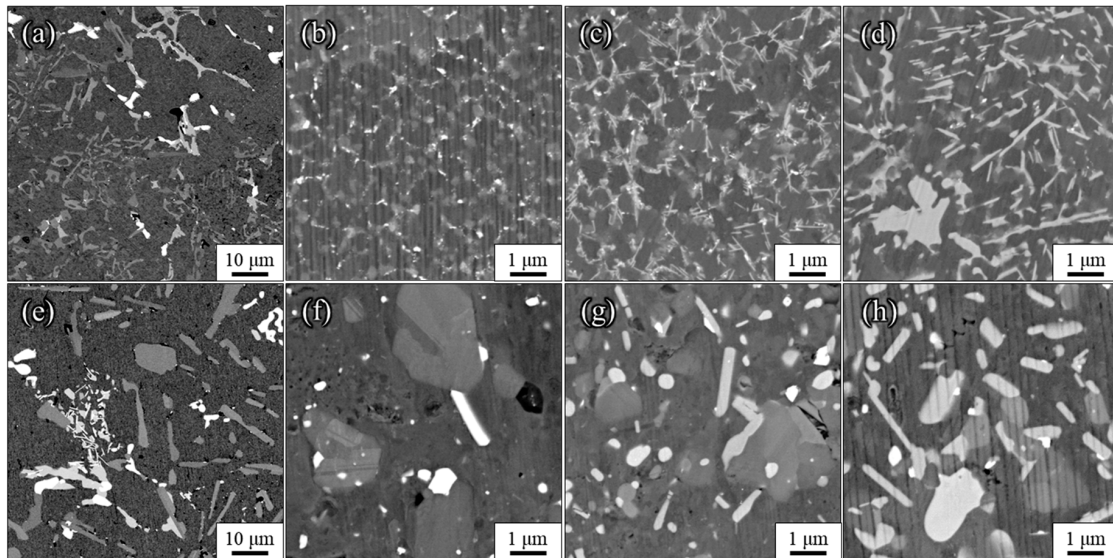


Figure 4. SEM-backscattered electron (BSE) images of cast and SLM alloys. (a) Cast-annealed Base, (b) SLM-annealed Base, (c) SLM-annealed Base + 3Fe, and (d) SLM-annealed Base + 5Fe, (e) Cast-T6 Base, (f) SLM-T6 Base, (g) SLM-T6 Base + 3Fe, and (h) SLM-T6 Base + 5Fe alloys.

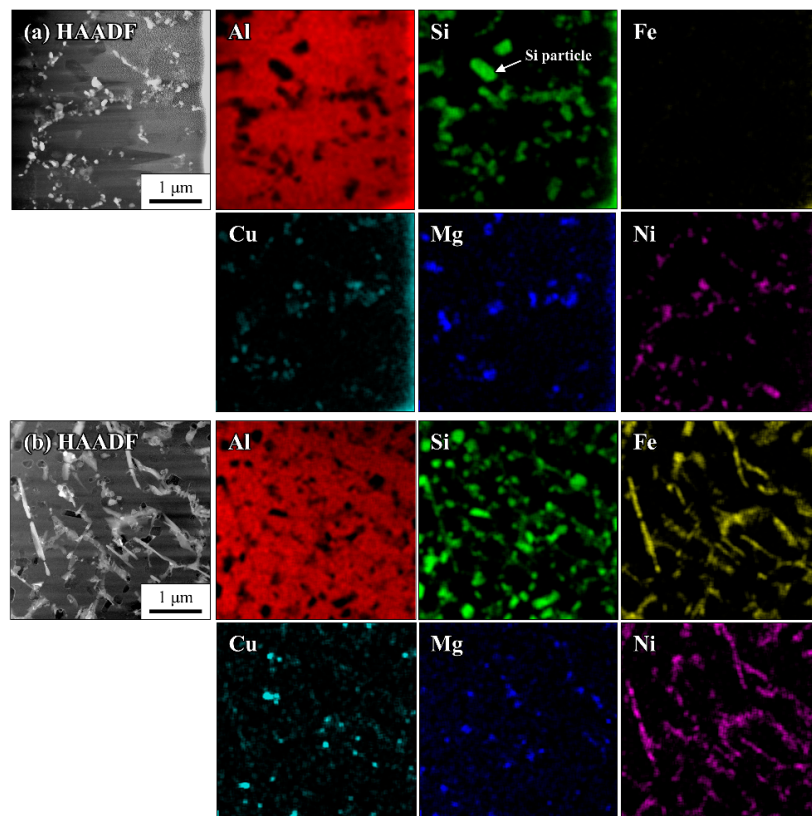


Figure 5. Scanning transmission electron microscopy–high-angle annular dark field (STEM-HAADF) images and corresponding energy-dispersive X-ray spectroscopy (EDS) element maps for (a) SLM-annealed Base and (b) SLM-annealed Base + 3Fe.

The Fe-Si-Ni particles in the Base + 3Fe alloy were finer than those in the Base + 5Fe alloy. Similar to the Si particles, the rod-shaped Fe-Si-Ni particles were coarsened by T6 treatment. T6 treatment coarsened the Si particles and destroyed the cellular structure of Si characteristic of the SLM materials. However, as shown in Figure 3, the UTS at 300 °C of the SLM-annealed Base alloy and SLM-T6 Base alloy were 77 and 69 MPa, respectively, which were not significantly different. Therefore, in contrast to the room-temperature strength [12], the cell structure of the Si particles did not contribute to an increase in high-temperature strength. This is also clear from that the UTS of the Base alloys produced by SLM and casting were almost the same in annealed condition. The ductility of the SLM-T6 Base alloy was improved compared with the cast Base alloys, though both alloys contained coarse Si particles. The Si particles in the SLM material that exhibited good ductility had an equiaxed shape, whereas those of the cast material had a Chinese script shape or rod shape. Therefore, it is considered that the equiaxial shape of the Si particles contributed to the improvement of the ductility of the SLM material.

In contrast to the Base alloy, the UTSs of the SLM-T6 Base + 3Fe and Base + 5Fe alloys at 300 °C were about 40% lower than the corresponding SLM-annealed alloys. The T6 treatment coarsened the Si and Fe-Si-Ni particles in the Fe-containing alloys. Because the high-temperature strength did not increase only with the fine cellular Si particles, we concluded that the fine dispersion of rod-shaped Fe-Si-Ni particles was the main reason that the SLM-annealed Base + 3Fe and Base + 5Fe alloys had excellent high-temperature strength. These fine particles were present even after annealing at 300 °C for 12 h; thus, they were stable at temperatures up to 300 °C and were useful for dispersion strengthening at high temperatures. In the annealed material, the rod-shaped Fe-Si-Ni particles formed cells together with Si particles. In future research, we intend to examine the effects of cellular particle distribution and cellular morphology on high-temperature strength.

4. Conclusions

- The Base alloy produced by SLM had superior ductility, although the tensile strength at 300 °C was similar to those manufactured by casting.
- The Base alloy manufactured by SLM had a fine cell structure of Si formed by the rapid solidification unique to this method. Although this microstructure did not increase the high-temperature strength of the material, it contributed to improving the ductility.
- Applying T6 treatment, which is commonly used for cast alloys, to the Base alloy produced by SLM destroyed the fine Si cell structure.
- The Fe-containing alloys produced by SLM showed better high-temperature strength while maintaining good ductility. This was caused by Fe being dispersed as fine Fe-Si-Ni particles due to the quenching solidification unique to SLM.

Author Contributions: S.Y. conducted original writing and data analysis; T.O. conducted experimental work; M.M. conducted data analysis; H.N. had a role in supervision; J.K. manufactured powder materials; M.A. conducted molding by selective laser melting.

Funding: This research received no external funding.

Conflicts of Interest: The authors declare no conflict of interest.

References

1. Hitzler, L.; Merkel, M.; Hall, W.; Ochsner, A. A review of metal fabricated with laser- and powder-bed based additive manufacturing techniques: process, nomenclature, materials, achievable properties, and its utilization in the medical sector. *Adv. Eng. Mater.* **2018**, *20*, 1700658. [[CrossRef](#)]
2. Herzog, D.; Seyda, V.; Wycisk, E.; Emmelmann, C. Additive manufacturing of metals. *Acta Mater.* **2016**, *117*, 371–392. [[CrossRef](#)]
3. Tang, M.; Pistorius, P.C.; Narra, S.; Beuth, J.L. Rapid solidification: Selective laser melting of AlSi10Mg. *JOM* **2016**, *68*, 960–966. [[CrossRef](#)]

4. Thijs, L.; Kempen, K.; Kruth, J.-P.; Humbeeck, J.V. Fine-structured aluminium products with controllable texture by selective laser melting of pre-alloyed AlSi10Mg powder. *Acta Mater.* **2013**, *61*, 1809–1819. [[CrossRef](#)]
5. Wu, J.; Wang, X.Q.; Wang, W.; Attallah, M.M.; Loretto, M.H. Microstructure and strength of selectively laser melted AlSi10Mg. *Acta Mater.* **2016**, *117*, 311–320. [[CrossRef](#)]
6. Liu, M.; Takata, N.; Suzuki, A.; Kobashi, M. Microstructural characterization of cellular AlSi10Mg alloy fabricated by selective laser melting. *Mater. Des.* **2018**, *157*, 478–491. [[CrossRef](#)]
7. Li, X.P.; Wang, X.J.; Saunders, M.; Suvorova, A.; Zhang, L.C.; Liu, Y.J.; Fang, M.H.; Huang, Z.H.; Sercombe, T.B. A selective laser melting and solution heat treatment refined Al–12Si alloy with a controllable ultrafine eutectic microstructure and 25% tensile ductility. *Acta Mater.* **2015**, *95*, 74–82. [[CrossRef](#)]
8. Prashanth, K.G.; Scudino, S.; Eckert, J. Defining the tensile properties of Al-12Si parts produced by selective laser melting. *Acta Mater.* **2017**, *126*, 25–35. [[CrossRef](#)]
9. Suryawanshi, J.; Prashanth, K.G.; Scudino, S.; Ecker, J.; Prakash, O.; Ramamurty, U. Simultaneous enhancements of strength and toughness in an Al-12Si alloy synthesized using selective laser melting. *Acta Mater.* **2016**, *115*, 285–294. [[CrossRef](#)]
10. Prashanth, K.G.; Scudino, S.; Klauss, H.J.; Surreddi, K.B.; Löber, L.; Wang, Z.; Chaubey, A.K.; Kühn, U.; Eckert, J. Microstructure and mechanical properties of Al–12Si produced by selective laser melting: Effect of heat treatment. *Mater. Sci. Eng. A* **2014**, *590*, 153–160. [[CrossRef](#)]
11. Fousova, M.; Dvorsky, D.; Vronka, M.; Vojtech, D.; Lejcek, P. The use of selective laser melting to increase the performance of AlSi9Cu3Fe alloy. *Materials* **2018**, *11*, 1918. [[CrossRef](#)]
12. Chen, B.; Moon, S.K.; Yao, X.; Bi, G.; Shen, J.; Umeda, J.; Kondoh, K. Strength and strain hardening of a selective laser melted AlSi10Mg alloy. *Scr. Mater.* **2017**, *141*, 45–49. [[CrossRef](#)]
13. Jung, J.-G.; Lee, S.-H.; Cho, Y.-H.; Yoon, W.-H.; Ahn, T.-Y.; Ahn, Y.-S.; Lee, J.-M. Effect of transition elements on the microstructure and tensile properties of Al12Si alloy cast under ultrasonic melt treatment. *J. Alloys Compd.* **2017**, *712*, 277–287. [[CrossRef](#)]
14. Liu, K.; Chen, X.-G. Improvement in elevated-temperature properties of Al–13% Si piston alloys by dispersoid strengthening via Mn addition. *J. Mater. Res.* **2018**, *33*, 3430–3438. [[CrossRef](#)]
15. Hernandez-Sandoval, J.; Garza-Elizondo, G.H.; Samuel, A.M.; Valtierra, S.; Samuel, F.H. The ambient and high temperature deformation behavior of Al–Si–Cu–Mg alloy with minor Ti, Zr, Ni additions. *Mater. Des.* **2014**, *58*, 89–101. [[CrossRef](#)]
16. De Luca, A.; Dunand, D.C.; Seidman, D.N. Microstructure and mechanical properties of a precipitation strengthened Al–Zr–Sc–Er–Si alloy with a very small Sc content. *Acta Mater.* **2018**, *144*, 80–91. [[CrossRef](#)]
17. Wang, L.; Makhlof, M.; Apelian, D. Aluminium die casting alloys: alloy composition, microstructure, and properties-performance relationships. *Int. Mater. Rev.* **1995**, *40*, 221–238. [[CrossRef](#)]
18. Cao, X.; Campbell, J. Morphology of β -Al5FeSi phase in Al–Si cast alloys. *Mater. Trans.* **2006**, *47*, 1303–1312. [[CrossRef](#)]
19. Dinnis, C.M.; Taylor, J.A.; Dahle, A.K. As-cast morphology of iron-intermetallics in Al–Si foundry alloys. *Scr. Mater.* **2005**, *53*, 955–958. [[CrossRef](#)]
20. Rajabi, M.; Vahidi, M.; Simchi, A.; Davami, P. Effect of rapid solidification on the microstructure and mechanical properties of hot-pressed Al–20Si–5Fe alloys. *Mater. Charact.* **2009**, *60*, 1370–1381. [[CrossRef](#)]
21. Prusa, F.; Vojtech, D. Mechanical properties and thermal stability of Al-23Si-8Fe-1Cr and Al-23Si-8Fe-5Mn alloys prepared by powder metallurgy. *Mater. Sci. Eng. A* **2013**, *565*, 13–20. [[CrossRef](#)]
22. Ma, P.; Jia, Y.; Prashanth, K.G.; Scudino, S.; Yu, Z.; Eckert, J. Microstructure and phase formation in Al-20Si-5Fe-3Cu-1Mg synthesized by selective laser melting. *J. Alloys Compd.* **2016**, *657*, 430–435. [[CrossRef](#)]
23. Simchi, A. Direct laser sintering of metal powders: Mechanism, kinetics and microstructural features. *Mater. Sci. Eng. A* **2006**, *428*, 148–158. [[CrossRef](#)]
24. Attar, H.; Ehtemam-Haghighi, S.; Kent, D.; Dargusch, M. Recent developments and opportunities in additive manufacturing of titanium-based matrix composites: A review. *Int. J. Mach. Tools Manuf.* **2018**, *133*, 85–102. [[CrossRef](#)]
25. Kasprzak, W.; Amirkhiz, B.; Niewczas, M. Structure and properties of cast Al–Si based alloy with Zr–V–Ti additions and its evaluation of high temperature performance. *J. Alloys Compd.* **2014**, *595*, 67–79. [[CrossRef](#)]
26. Wang, E.R.; Hui, X.D.; Chen, G.L. Eutectic Al–Si–Cu–Fe–Mn alloys with enhanced mechanical properties at room and elevated temperature. *Mater. Des.* **2011**, *32*, 4333–4340. [[CrossRef](#)]

27. Mohamed, A.M.A.; Samuel, F.H.; Al kahtani, S. Microstructure, tensile properties and fracture behavior of high temperature Al–Si–Mg–Cu cast alloys. *Mater. Sci. Eng. A* **2013**, *577*, 64–72. [[CrossRef](#)]
28. Shaha, S.K.; Czerwinski, F.; Kasprzak, W.; Friedman, J.; Chen, D.L. Improving High-Temperature Tensile and Low-Cycle Fatigue Behavior of Al-Si-Cu-Mg Alloys Through Micro-additions of Ti, V, and Zr. *Metall. Mater. Trans. A* **2015**, *46A*, 3063–3078. [[CrossRef](#)]
29. Khalifa, W.; Samuel, A.M.; Samuel, F.H.; Doty, H.W.; Valtierra, S. Metallographic observations of β -AlFeSi phase and its role in porosity formation in Al–7%Si alloys. *Int. J. Cast Met. Res.* **2006**, *19*, 156–166. [[CrossRef](#)]
30. Wang, Y.M.; Voisin, T.; McKeown, J.T.; Ye, J.; Calta, N.P.; Li, Z.; Zeng, Z.; Zhang, Y.; Chen, W.; Roehling, T.T.; et al. Additively manufactured hierarchical stainless steels with high strength and ductility. *Nat. Mater.* **2018**, *17*, 63–70. [[CrossRef](#)]



© 2019 by the authors. Licensee MDPI, Basel, Switzerland. This article is an open access article distributed under the terms and conditions of the Creative Commons Attribution (CC BY) license (<http://creativecommons.org/licenses/by/4.0/>).